Composites: Part B 66 (2014) 381–387

Contents lists available at ScienceDirect

Composites: Part B

journal homepage: www.elsevier.com/locate/compositesb

Evaluation of thermal barrier effect of ceramic microparticulate surface coatings on glass fibre-reinforced epoxy composites

Baljinder K. Kandola *, Piyanuch Luangtriratana

Institute for Materials Research and Innovation, University of Bolton, Deane Road, Bolton BL3 5AB, UK

ARTICLE INFO

Article history:
Received 3 February 2014
Received in revised form 30 April 2014
Accepted 3 June 2014
Available online 11 June 2014

Keywords:
A. Laminates
A. Polymer-matrix composites (PMCs)
B. Thermal properties
E. Surface treatments

ABSTRACT

In this work, three commercially available ceramic particles have been used as thermal barrier coatings on glass fibre-reinforced epoxy composites. The coatings have been prepared by dispersing 70 wt.% ceramic particle in 30 wt.% flame retarded epoxy resin. The thermal barrier efficiency of the coatings on the composites has been studied in terms of temperature gradient through the thickness of the sample while the surface is exposed to a radiant heat of varying heat fluxes. The tests have been performed in a cone calorimeter by inserting two thermocouples, one underneath the coating and the other on the reverse side of the sample during the experiments. This also allowed evaluating their flammability performance.

1. Introduction

Thermal barrier coatings (TBCs) are usually applied to metallic surfaces of components operating at elevated temperatures, such as aircraft and rocket engines, industrial gas turbines, marine propulsions, pistons and cylinders in diesel engines, compressors, chemicals and petroleum plants. The metals usually used in these applications vary from superalloys (various combinations of Fe, Ni, Co, and Cr), titanium alloys, niobium alloys and steel. The TBCs are comprised of ceramic particles of low thermal conductivity (e.g. yttria stabilised zirconia, thermal conductivity ~1 W/m K), which can sustain a significant temperature gradient between the load bearing metallic part and the exposed coated surface, hence extending the part's life span. These coatings are also required to protect the metal components from oxidation and corrosion. A typical thermal barrier coating on the metallic substrate consists of three layers [1]. The first layer is the bond coat and as the name implies, it bonds the coating to the substrate. The bond coat is usually a metallic layer made of a nano-structured ceramic–metallic composite, 75–125 μm thick [2]. Two types of materials are used for bond coats, NiCoCrAlY system or Pt-modified diffusion aluminide type [3]. This layer also helps in generating the second coating layer of thermally grown ceramic oxide, produced when the coating is subjected to a high temperature. Nanoparticles of alumina oxide and nitrides are usually added to the bond coat, which catalyse the thermal growth of oxide layer. This thin (3–10 μm) thermally grown aluminium rich oxide layer's role is to inhibit the oxidation of the bond coat. The last layer is ceramic top coat, usually made of yttria stabilised zirconia and of about 100–375 μm (depending upon the application) thickness. This acts as a thermal insulator and protects the underlying structures from thermal stresses. MgO, CaO, and CeO_2 are other oxide stabiliser used for ZrO_2. The thermal barrier coatings can be fabricated either by dry route or soft chemical process. The dry processes include Air Plasma Spray (APS), Low Pressure Plasma Spray (LPPS) or the Electron Beam Physical Vapour Deposition (EB-PVD), Vacuum Plasma Spray (VPS) or High Velocity Oxygen Fuel (HVOF) [4–6]. For chemical route, sol–gel deposition is used [7].

Although most of these types of ceramic-coatings are applied to metallic parts, due to replacement of metallic parts by fibre-reinforced composites, their use in composites can also be very advantageous. However, most of the techniques of application on metallic substrate require very high temperatures, even in sol–gel technique after dip coating the substrate in a solution (e.g. yttria stabilised zirconia slurry) the heat treatment is performed at 950–1150 °C [8]. Hence there is a need to explore alternative methods of application at temperatures below the decomposition temperature of the organic resin component of the composites.

Fibre-reinforced composites due to their high mechanical strength can serve the same purpose as metals for structural applications but they respond very differently to high temperatures and fire [9]. At temperatures below the glass transition temperature of the resin, there is not much effect on mechanical properties. On

* Corresponding author. Tel.: +44 1 204 903517.
E-mail address: B.Kandola@bolton.ac.uk (B.K. Kandola).

http://dx.doi.org/10.1016/j.compositesb.2014.06.002
1359-8368/

reaching the glass transition temperature (150–220 °C, depending upon the resin type), the composite laminate starts losing mechanical properties, as high as 50% of the original values [10,11], which however, can be regained on cooling down the laminate back to ambient temp [9]. This behaviour is maintained until the temperature reaches the decomposition temperature of the resin (>300 °C), when the resin matrix begins to decompose into volatile combustible gases, which may ignite and burn the rest of the matrix resin, resulting in complete loss of mechanical integrity of the laminate [9,12]. Hence, any thermal barrier coating should be effective enough to protect the resin from ignition. This work explores the thermal barrier efficiency of some traditional ceramic components used for metals. Low melting glass is also explored, which on heating forms a thin silica layer on the surface and is known to provide passive fire protection [13].

2. Experimental

2.1. Materials

2.1.1. Glass fibre-reinforced epoxy (GRE) composite

Epoxy resin system: epoxy phenol novolac resin (Araldite LY5052, Huntsman) and cycloaliphatic polyamine-2,2-dimethyl-4,4-methylene bis cyclohexylamine hardener (Aradur HY 5052, Huntsman).

Glass fibre: Woven roving glass fibre of E-glass type (300 g/m^2, Glasplies).

2.1.2. Ceramic micro-particles for surface coatings

Ceepree (Ce): low-melting silicate glass (M.&C.T Ltd., UK). Thermal conductivity of this product is not known, typical value for common glass formulations is ~1.8–2.0 W/(m K) [14].

Zirconium oxide (Zr): Aqueous dispersion of yttria doped zirconia, consists of 91–93% zirconium oxide and 7–9% yttrium oxide (XZO1357, Mel Chemical, UK). The particles were obtained by evaporating water at 60 °C in an oven for 24 h. The residue was grinded with mortar and pestle. Thermal conductivity of these particles is not known, typical value for yttria stabilised zirconia is ~1.5–2.0 W/(m K) [15].

Recoxit (Re): Al_2TiO_5 (Ohcera. Co., Ltd., Japan). Thermal conductivity ~1.5–2.0 W/(m K) [16].

2.1.3. Binder

Flame retarded epoxy: epoxy resin (Araldite LY5052) containing 10 wt.% DOPO (dihydro-oxa-phosphaphenanthrene-oxide, TCI Tokyo Kasei, Japan).

2.2. Sample preparation

2.2.1. Glass fibre reinforced epoxy (GRE) composite laminate

Eight pieces of 300 mm × 300 mm woven E-glass fabric were used for composite laminate preparation, with the ratio of 50 wt.% glass fibre and 50 wt.% resin matrix. The GRE composites laminate was fabricated using a hand lay-up method by impregnating each glass fabric layer with the resin, vacuum bagging and curing at room temperature for at 24 h, and then post-curing at 80 °C for 6 h.

2.2.2. Micro-particulate ceramic coatings on GRE composite

Three commercially ceramic particles were used to prepare the ceramic surface coatings of approximately 1 mm. thicknesses on pre-prepared (cured) GRE composite by dispersing the ceramic particles (70 wt.%) and the flame retarded epoxy resin binder (30 wt.%) in methyl ethyl ketone (MEK, 50 wt.% w.r.t mixture of flame retarded epoxy resin and ceramic particle). The suspension was stirred with a mechanical stirrer for 10 min. The hardener, Aradur HY5052 (30 wt.% w.r.t. flame retarded epoxy resin) was added and continued to stir for another 5 min.

The master laminate plate as discussed in Section 2.2.1 was cut into samples of 75 × 37 mm and each sample was individually coated by the coating mixtures of Ceepree, Zirconia and Recoxit. Samples are named as GRE-Ce, GRE-Zr and GRE-Re, respectively. These three coatings were applied by a roller and paint brush to obtain ~1 mm thicknesses. Since each specimen was individually coated, there is a small variation in mass of the coating and the coating thickness (see Table 1). The samples were then cured at room temperature for 12 h and post-cured at 80 °C for 6 h.

2.3. Physical and morphological characterisation of coatings

All samples were weighed before and after coating application and the wt.% clay deposited on the surface was calculated. The thicknesses of coatings were obtained from the difference of thicknesses of coated and uncoated samples, measured using a digital caliper. The morphologies of coatings were studied by using scanning electron microscopy (SEM, Hitachi Technologies Model 3400) with accelerating voltage capacity 1–30 kV and magnification ranges between 10× and 300,000× at 30 kV providing resolution down to 10 μm. The particle sizes of the Ceepree, Recoxit and zirconia were also determined from SEM images by using an image analysis software (Image J, National Institute of Health/USA) [17]. Measurements were performed on 20 particles chosen from each of five different regions of the micrographs to ensure adequate statistical confidence.

2.4. Flammability and thermal barrier study

The flammability of all GRE composite laminates with/without three ceramic surface coatings samples was evaluated in a cone calorimeter (Fire Testing Technology, UK). Three specimens of each of control (without surface coating) and with surface coated samples (see Table 1) were tested by exposing them to various heat fluxes ranging from 20 to 50 kW/m^2 in the horizontal mode with an ignition source. While the test specimens used in this study have relatively shorter dimensions (75 mm × 37 mm) than those recommended in ISO 5660 standard (100 mm × 100 mm), the results are discussed in comparative terms. Furthermore, previous research in our research facilities [18] showed that the reduction in the surface area of the cone calorimetry test specimens does not significantly affect their fire behaviour.

In order to study thermal barrier properties and thermal resistance of each type of ceramic coatings, three *K*-type thermocouples were placed, one on top of the surface coating and two on reverse side of samples. The thermocouples recorded temperature as a function of time for duration of exposure to various heat fluxes.

3. Results and discussion

3.1. Surface characterisation

The surface of the GRE composite laminate is very smooth and featureless as seen from Fig. 1. With different ceramic particles, 0.9–1.1 mm thick coatings could be deposited on the surface of the laminates. The exact thickness, mass of each coating and percent ceramic particles deposited on the surface of laminates are given in Table 1. Since each laminate was individually coated, there is small variation in mass and thickness in different laminates of one type, the variation in values is also given in Table 1. SEM characterisation of the surfaces of coated samples show that the particles are well dispersed in the resin of the coatings, i.e., there are no aggregates. The distribution of particles depends on the

Table 1
Physical properties of GRE composite laminates with/without coatings.

Sample	Ceramic particle size (μm)	Coating thickness (mm)	Mass of coating (g)	Mass of ceramic particles in coating (g)	Ceramic particle deposited (wt.%, w.r.t laminate)
Control	–	–	–	–	–
GRE-Ce	11 ± 1	1.09 ± 0.07	4.30 ± 0.17	3.01 ± 0.12	35 ± 2
GRE-Re	4 ± 2	0.89 ± 0.06	4.22 ± 0.04	2.95 ± 0.03	34 ± 1
GRE-Zr	19 ± 4	0.94 ± 0.21	4.78 ± 0.21	3.35 ± 0.39	40 ± 1

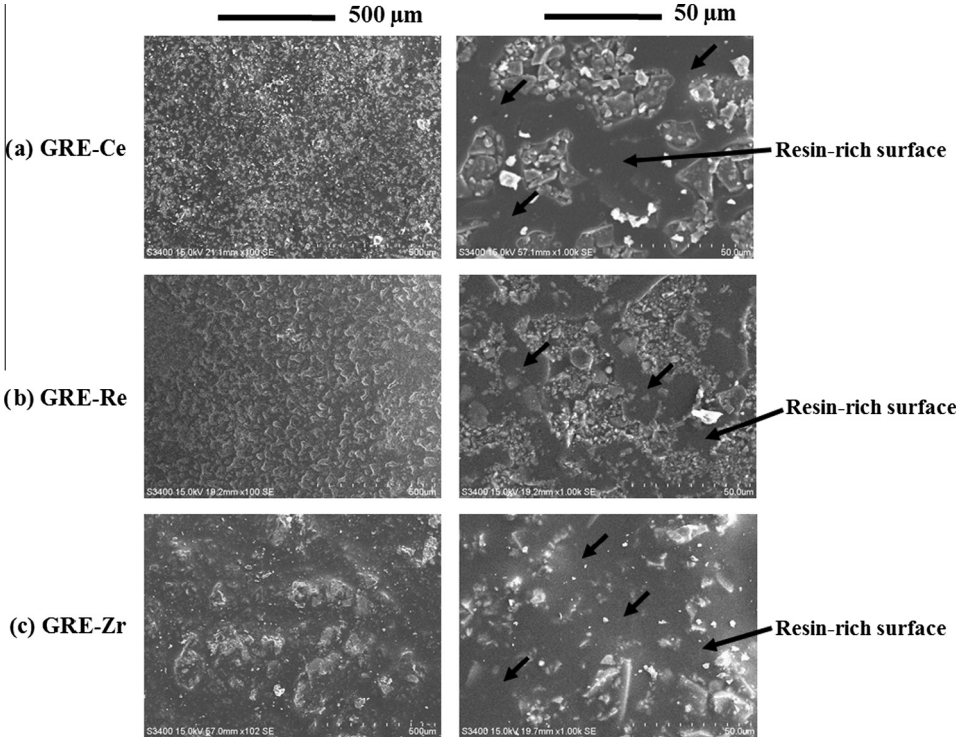

Fig. 1. SEM images of (a) GRE-Ce, (b) GRE-Re and (c) GRE-Zr.

particle size of each ceramic type. As can be seen in Table 1, the average particle size of Recoxit is smaller (~4 μm) compared to Ceepree (~11 μm) and zirconia (~19 μm), which results in better particle distribution in the coating of GRE-Re than GRE-Ce and GRE-Zr (Fig. 1(a–c)). However, the ceramic particles do not completely cover the surfaces for these three coated samples, which is probably due to the coating application method, i.e. using paint brush/roller techniques allows a good distribution of the particles on the GRE laminate surfaces, although some resin binder is exposed on the surface.

3.2. Flammability behaviour of glass fibre-reinforced epoxy composite (GRE)

The flammability properties of the GRE composites without/with surface coatings were evaluated at different heat fluxes (20, 30 40 and 50 kW/m^2) using a cone calorimeter. For a given composite of defined thickness, the flammability is determined by the intensity of the fire, i.e. the incident heat flux. While most of the medium and large scale fire tests involve heat sources or 'simulated fires' having constant and defined fluxes, in real fires, heat fluxes may vary. For example, a domestic room filled with burning furniture at the point of flashover presents a heat flux of about 50 kW/m^2, whereas larger building fires present fluxes as high as 100 kW/m^2 and hydrocarbon fuel "pool fires" may exceed 150 kW/m^2. In this work, heat fluxes representing low, moderate and room fire conditions (20–50 kW/m^2) were chosen, where the maximum surface temperature reached on the surface can vary from ~370 (at 20 kW/m^2) to ~570 °C (at 50 kW/m^2). The heat release rate (HRR) curves as a function of exposure time at different heat fluxes are shown in Fig. 2 and all derived results are presented in Table 2. In this section, the flammability behaviour of GRE composites coated with different microparticulate ceramics are discussed, firstly, at one heat flux (50 kW/m^2) in order to observe the effect of different components on overall fire performance of the composites and secondly, at different heat fluxes in order to observe the effect of external heat energy input.

At 50 kW/m^2 the control GRE sample ignited after 31 s of continued exposure to the heat and spark ignition. Fig. 2(d) shows an intense single peak of HRR of 695 kW/m^2 at 90 s. The process of heat release of control sample finished within 160 s (see Table 2). The increase of the heat release rates can be explained as the increase in the quantity of combustible volatiles during the heat exposure, which on reaching a critical mass flux ignite with the spark ignition and as the combustible volatiles are burnt out, the HRR starts decreasing. The samples coated by Ceepree, Recoxit and zirconia showed similar single peak HRR-curves as control sample, but of less intensity representing lower heat release rate, which signifies the low rate of generation of combustible volatiles after the resin binder in the coating ignited leading to burning of all of the resin in the composite. The ignition occurs due to the exposed resin on the surface as seen from Fig. 1(a–c), i.e., the

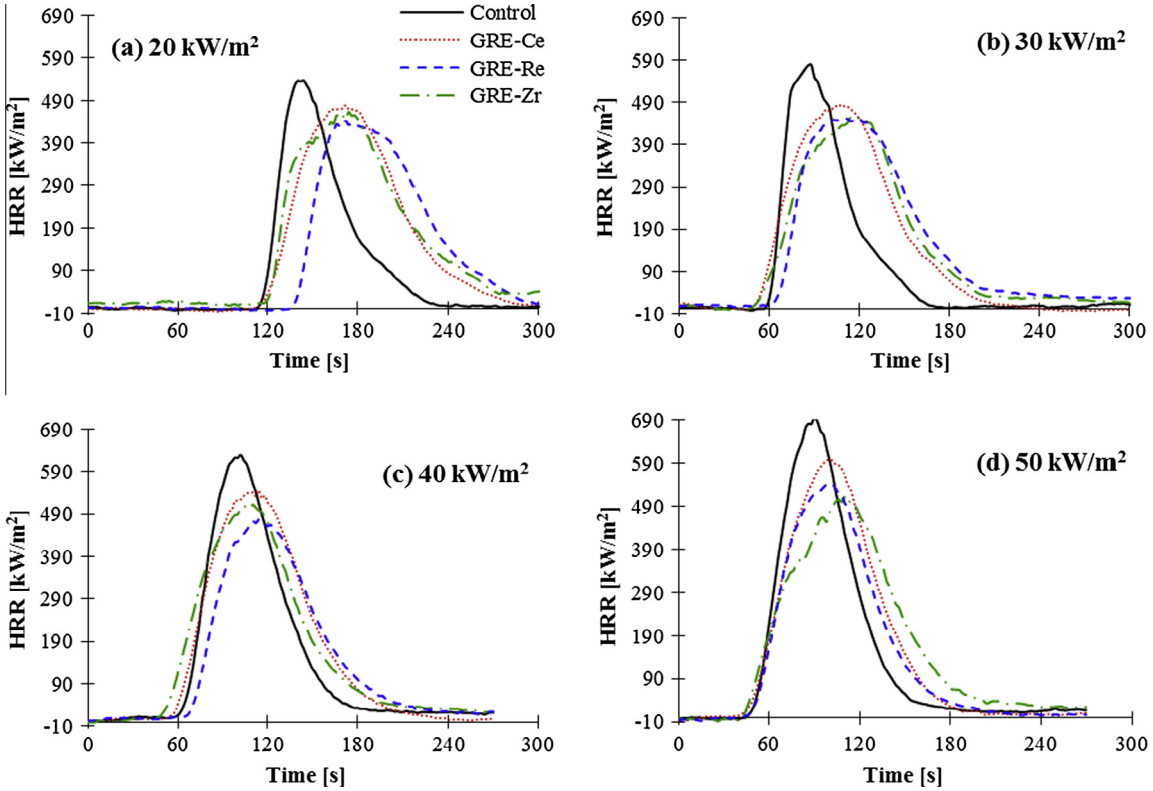

Fig. 2. The HRR versus time curves at (a) 20, (b) 30, (c) 40 and (d) 50 kW/m^2 for control, GRE-Ce, GRE-Zr and GRE-Re samples.

Table 2
Cone calorimetric data for surface coated GRE composite samples exposed to 20, 30, 40 and 50 kW/m^2 heat fluxes with an ignition source.

Sample	Heat fluxes (kW/m^2)	TTI (s)	FO (s)	T_{ign}[a] (°C)	PHRR (kW/m^2)	Time to PHRR (s)	THR (MJ/m^2)	Total smoke release (1)	FIGRA[b] (kW/m^2 s)
Control	20	118 ± 1	234 ± 1	338 ± 2	538 ± 39	142 ± 2	26.5 ± 2.5	889 ± 40	3.8 ± 0.3
	30	62 ± 1	178 ± 1	394 ± 8	571 ± 14	83 ± 3	30.8 ± 2.4	961 ± 15	6.8 ± 0.5
	40	45 ± 1	164 ± 1	424 ± 4	642 ± 15	100 ± 2	37.5 ± 3.0	1464 ± 17	6.4 ± 0.3
	50	31 ± 1	160 ± 2	466 ± 7	695 ± 53	90 ± 1	38.7 ± 3.0	1676 ± 81	7.7 ± 0.6
GRE-Ce	20	122 ± 6	284 ± 4	348 ± 3	481 ± 15	170 ± 8	38.0 ± 0.6	1367 ± 13	2.8 ± 0.1
	30	55 ± 4	197 ± 3	359 ± 4	501 ± 14	108 ± 10	38.7 ± 1.1	1364 ± 93	4.7 ± 0.6
	40	38 ± 1	183 ± 1	385 ± 2	553 ± 23	110 ± 8	41.4 ± 0.2	1889 ± 173	5.0 ± 0.2
	50	29 ± 1	172 ± 1	407 ± 5	597 ± 22	100 ± 1	41.7 ± 2.8	1877 ± 18	5.9 ± 0.2
GRE-Re	20	140 ± 2	293 ± 1	332 ± 1	447 ± 20	179 ± 7	37.3 ± 3.2	1470 ± 104	2.5 ± 0.2
	30	68 ± 8	207 ± 5	358 ± 4	458 ± 11	119 ± 7	40.2 ± 1.9	1406 ± 122	3.9 ± 0.3
	40	49 ± 1	182 ± 1	397 ± 3	478 ± 13	116 ± 6	41.6 ± 0.3	1713 ± 43	4.1 ± 0.3
	50	30 ± 1	170 ± 3	418 ± 4	544 ± 4	100 ± 2	42.8 ± 2.1	1855 ± 111	5.4 ± 0.1
GRE-Zr	20	123 ± 4	279 ± 2	346 ± 2	463 ± 27	174 ± 4	41.0 ± 2.7	1072 ± 11	2.3 ± 0.3
	30	61 ± 7	218 ± 1	351 ± 7	470 ± 2	121 ± 7	40.1 ± 1.5	1323 ± 25	3.9 ± 0.2
	40	32 ± 1	181 ± 3	373 ± 4	512 ± 1	108 ± 2	41.9 ± 3.7	1637 ± 35	4.7 ± 0.1
	50	24 ± 1	175 ± 1	422 ± 3	511 ± 49	114 ± 4	43.5 ± 0.5	1826 ± 57	4.1 ± 0.6

[a] T_{ign} is the surface temperature at TTI, measured by thermocouple inserted on the surface of the laminate.
[b] FIGRA index = PHRR/time-to-PHRR (kW/m^2 s).

ceramic layer is not fully covering the surface to provide an effective barrier layer for a period of time. The reproducibility of the coated samples can be seen from Table 2. The slight variations in results are due to different coating thicknesses (Table 1), plus the general variation in cone experimental results.

For a good flame retardant system the cone results are demonstrated by increase in time-to-ignition (TTI) (preferably no ignition) and reduction in peak heat release rate (PHRR), total heat release (THR), mass loss rate and smoke production. Surface coatings working as passive fire protection show their thermal barrier efficiency by decrease in PHRR and increase in time-to-PHRR, whereas the burn time, THR and smoke production are increased due to slow and prolonged burning [19,20].

In this case as seen from Table 2, there is no effect on TTI and in some cases there is slight reduction. The reduction in TTI can be explained due to the phosphorus-based flame retardant in the binder resin decomposes earlier (<250 °C) than the epoxy binder resin. The O═P—O bond in DOPO flame-retarded epoxy is less stable than the common C—C bond in pure epoxy [21], the released phosphoric acid then reacts with epoxy group and changes the decomposition mechanism of the latter to produce more char formation. In this case the concentration of flame retarded resin in the composite is too low to show this as a significant effect.

The improvement in fire resistance can be seen by the reduction in PHRR of coated samples compared to the control sample. At 50 kW/m^2, these three ceramic coatings could reduce PHRR values

by 14–26% and prolong time-to-PHRR compared to the control sample (PHRR values of 695 kW/m^2). This can be explained by the fact that Ceepree, Recoxit and zirconia particles have low thermal conductivity values (~1.5–2 W/(m K)), and so act as thermal insulators and prevent the diffusion of all the volatiles generated during combustion of the resin. Based on reduction in PHRR, the samples can be ranked as:

$$\text{GRE-Zr}(511\ \text{kW/m}^2) < \text{GRE-Re}(544\ \text{kW/m}^2) < \text{GRE-Ce}(597\ \text{kW/m}^2)$$

The better performance of zirconia particle can be explained due to the highest percentage of particle deposited is in GRE-DP/Zr (~40%) compared to other two coated samples (see Table 1). The FIGRA (Fire Growth Rate Index), which indicates the burning propensity of a material, is an important parameter as it is calculated from the ratio of maximum quotient of HRR(t) and time-to-PHRR which often equals to PHRR/time-to-PHRR in a cone calorimeter [22]. Lower the FIGRA value, lower the fire growth in a material. As seen from Table 2, the FIGRA of GRE-Zr has the lowest value (4.1 kW/m^{2}s), followed by GRE-Re (5.4 kW/m^{2}s) and GRE-Ce (5.9 kW/m^{2}s), which are significantly less than that of the control sample (7.7 kW/m^{2}s).

The mass loss curves shown in Fig. 3 show that although the coated samples start losing mass slightly earlier than the control sample, the mass loss rate is reduced. The residual contents at the end of the experiments represent the ceramic particles left on the surface as shown in Fig. 4. As can be seen from Fig. 4(a) that the resin matrix in control sample is totally burned out and only glass fibres can be seen with no char in between. For all coated samples, however, thin ceramic layers are left on the surface. In Fig. 4(b) a compact glassy silicate residual surface layer can be observed, which is due to silicate glass melting (the melting temperature is ~350 °C [23]), flowing and setting into a hard glassy structure [13]. This can be clearly seen from the SEM image in Fig. 5. This silicate layer acts as an insulator on the surface of the material to block heat flow. GRE-Zr sample contains 3–7% yttria doped zirconia, which has very high melting point (2600–2700 °C) [24]. The zirconia particle layer was left at the end of experiment (see Fig. 4(c)), with no mechanical coherence. Similarly in GRE-Re sample, which contains Al_2TiO_5 (melting point >1800 °C) [16], the Al_2TiO_5 particle residue can be seen on the surface in Fig. 4(d). In both cases as there was no binder left to hold the ceramic particles on the laminate, the particles were easily blown off and no SEM images could be obtained.

Although, these three coatings helped in reducing the PHRR and FIGRA values of the composite, the THR increased due to extra resin in the coating (see Table 2). Moreover, the application of these coatings increased total smoke release (TSR) values compared to un-coated sample, which is due to slow and prolonged burning.

From these results at 50 kW/m^2 heat flux, it can be concluded that the ceramic coatings are not very effective in reducing TTI of composite, due to resin binder in the coating, but provided an insulative thermal barrier property to reduce PHRR values, decrease FIGRA index and delay time-to-PHRR, which indicate the improvement of fire resistance performance of composite materials. The coatings could also retard mass loss rate compared to the control sample, which indicates that the ceramic particles mainly act by physical means, i.e. via their low thermal conductivity helps in reducing the heat transfer from the surface to the underlying structure. The coatings had no effect on residual char at the end of experiment (see Fig. 3), confirming passive action, i.e. it slows down the mass loss but does not prevent it.

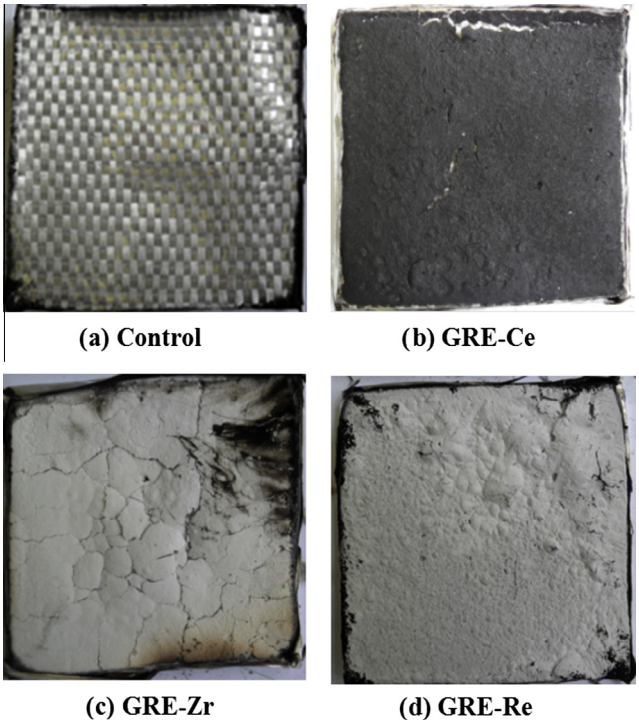

Fig. 4. Digital image of charred residues of control, GRE-Ce, GRE-Re and GRE-Zr samples after exposure to 50 kW/m^2.

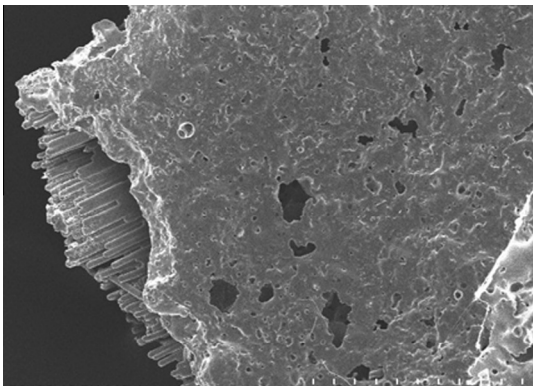

Fig. 5. SEM image of charred residues of GRE-Ce sample after exposure to 50 kW/m^2.

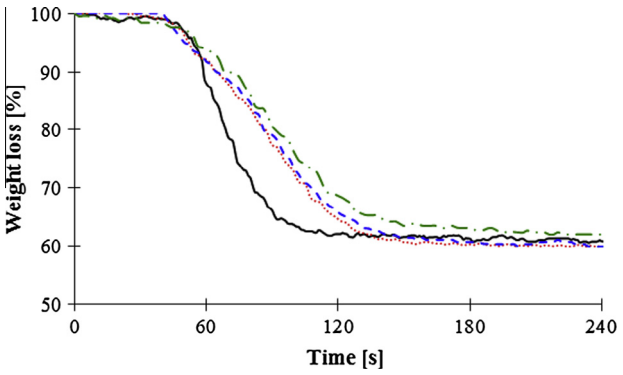

Fig. 3. Mass loss versus time curves for control, GRE-Ce, GRE-Zr and GRE-Re samples at 50 kW/m^2.

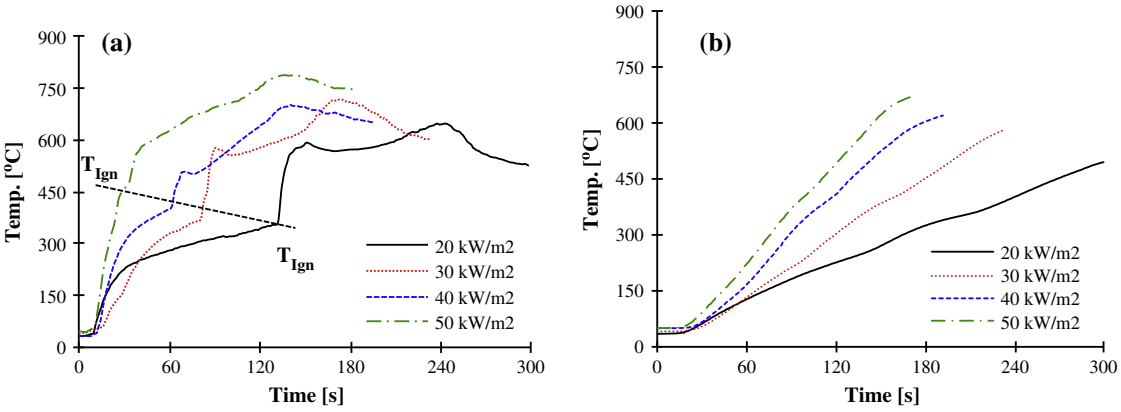

Fig. 6. (a) Surface and (b) reverse side temperatures of GRE-Zr as a function of time at different heat fluxes.

3.3. The effect of varying heat fluxes on flammability of GRE composites

The effect of heat fluxes ranging from 20–50 kW/m^2 on heat release rate of different samples are resented in Fig. 2 and cone parameters demonstrating the thermal barrier properties are presented in Table 2. At 20 kW/m^2 heat flux the control sample ignited at 118 s and has PHRR value of 538 kW/m^2 at 142 s. With increasing heat flux from 20 to 50 kW/m^2, the value of PHRR increases, whereas TTI and time-to-PHRR decrease, which result in an increase in FIGRA values of control sample. The total burn out time of the control sample decreases with increasing heat flux as expected (see Table 2). The effect of external heat flux on these parameters is as expected. With increasing heat flux the energy impact per time in the sample increases as evidenced by the increase in surface temp in Fig. 6. This results in increase in heating rate of the sample, decomposing the resin earlier and reaching the critical mass flux of volatiles for ignition to occur earlier, hence decreasing the TTI. After ignition, the decomposition rate of the resin producing combustible volatiles increases, resulting in increase in heat release rate (PHRR in Table 2) and the time for complete decomposition of the resin (FO in Table 2) is reduced [25]. This also results in increase in THR.

Similar trends for TTI, PHRR and time-to-PHRR with increasing heat fluxes can be seen for all coated samples as well. Moreover, a significant difference from 20 to 30 kW/m^2 heat flux can be seen, but not much from 40 to 50 kW/m^2.

As can be seen from Table 2, GRE-Ce and GRE-Zr samples had similar TTI as the control sample at 20 kW/m^2, but sample GRE-Re had longest ignition time of 140 s. As the heat flux increased, the ignition time of GRE-Ce, GRE-Zr and GRE-Re samples decreased and became lower than that of the control sample. THR values for all coated samples are higher than the control samples at respective heat fluxes (see Table 2). These results are consistent with the results in Section 2.1 that these ceramic coatings had no significant effect on reducing time-to-ignition of the composite but increased THR. However, these three coatings could decrease PHRR and FIGRA values by up to 20% and 50%, respectively compared to control sample at 20 and 30 kW/m^2 heat flux. In general the effectiveness of these three coatings can be ranked as:

GRE-Re > GRE-Zr > GRE-Ce

These results also suggest that all coatings at lower heat fluxes, 20 and 30 kW/m^2 showed better thermal barrier performance than at high heat fluxes, i.e. $\geqslant$40 kW/m^2. Moreover, the zirconia and Recoxit ceramic particles showed better thermal barrier performance than Ceepree at respective heat fluxes. This is due to difference in the thermal conductivity values and percent particle deposition of these three powders in the coatings, as discussed earlier.

Table 3
The time required to reach selected temperature at the reverse side for Control, GRE-Ce, GRE-Zr and GRE-Re samples at different heat fluxes.

Heat fluxes (kW/m^2)	Sample	The time to reach selected temperature at reverse side (s)							
		180 °C		250 °C		400 °C		500 °C	
20	Control	62 ± 6	–	96 ± 9	–	161 ± 7	–	207 ± 13	–
	GRE-Ce	105 ± 8	(+43)	158 ± 7	(+62)	202 ± 8	(+41)	259 ± 6	(+52)
	GRE-Re	109 ± 6	(+47)	165 ± 12	(+69)	229 ± 11	(+68)	281 ± 18	(+74)
	GRE-Zr	106 ± 5	(+44)	147 ± 16	(+51)	238 ± 4	(+77)	260 ± 2	(+53)
30	Control	56 ± 2	–	73 ± 2	–	107 ± 0	–	132 ± 4	–
	GRE-Ce	69 ± 4	(+13)	98 ± 8	(+25)	137 ± 11	(+30)	180 ± 14	(+48)
	GRE-Re	75 ± 4	(+19)	100 ± 6	(+27)	158 ± 7	(+51)	201 ± 7	(+69)
	GRE-Zr	78 ± 11	(+22)	104 ± 5	(+31)	159 ± 10	(+52)	201 ± 8	(+69)
40	Control	46 ± 4	–	65 ± 4	–	100 ± 5		122 ± 5	
	GRE-Ce	55 ± 6	(+9)	75 ± 8	(+10)	109 ± 9	(+9)	140 ± 10	(+18)
	GRE-Re	57 ± 3	(+11)	77 ± 4	(+12)	113 ± 14	(+13)	143 ± 14	(+21)
	GRE-Zr	59 ± 3	(+13)	78 ± 4	(+13)	118 ± 4	(+18)	149 ± 4	(+27)
50	Control	43 ± 2	–	57 ± 4	–	86 ± 3	–	107 ± 8	–
	GRE-Ce	47 ± 7	(+4)	62 ± 8	(+5)	96 ± 7	(+10)	123 ± 8	(+16)
	GRE-Re	50 ± 3	(+7)	64 ± 4	(+7)	99 ± 6	(+13)	124 ± 3	(+17)
	GRE-Zr	57 ± 6	(+14)	73 ± 6	(+16)	116 ± 5	(+30)	147 ± 5	(+40)

'(+)' Indicates increasing in time to reach at given temperature respective to control sample.

3.4. Thermal barrier properties

Thermal barrier effect of these coatings could be investigated by the temperature profiles of the surface (T_S) and the reverse side (T_R) of the laminate, which were recorded by *K*-type thermocouples during the cone experiments at different heat fluxes, shown for one sample in Fig. 6. The time taken for the insulated/reverse surface of the exposed GRE laminates to reach glass transition temperature of a typical epoxy resin (180 °C), onset of decomposition temperature (250 °C), temperature around which maximum degradation/oxidation of char occurs (400 and 500 °C) are given in Table 3. It should be noted that these are the approximate temperatures for a range of different epoxy type, not in particular for the resin used in this case. As can be seen from Table 3, the ceramic coating help in delaying the time to reach any particular temperature and this effect is more pronounced at low, 20 and 30 kW/m^2 heat flux, as the heat flux increases the difference becomes less. It can be seen that the order of efficiency with respect to thermal protection is: GRE-Zr ≈ GRE-Re > GRE-Ce.

This shows that when exposed to low heat fluxes, the ceramic particles act as effective thermal barriers, however, when the surface resin gets ignited, they do not provide effective fire protection.

4. Conclusions

In this work the thermal barrier effect of ceramic coatings on glass-reinforced epoxy composites on exposure to radiant heat fluxes between 20 and 50 kW/m^2 has been studied. From the results it can be concluded that these ceramic particle coatings containing the DOPO flame retarded epoxy resin binder can provide insulative thermal barrier property in terms of reducing PHRR values, decrease in FIGRA index and delay in time-to-PHRR values. However, the flammable resin-rich surface caused decrease in time-to-ignition and increase in THR of the laminates. Therefore, in the surface coating layer flame retardant additives/chemicals should be present which can delay/stop ignition of the resin binder, as these ceramic particles act only as thermal insulators, not flame retardants. In terms of heat penetration, at low heat fluxes all ceramic coatings provided effective thermal barrier/insulative char layers, which helped to delay the heat transfer from surface to underlying layers, measured as slower rise in temperature and increasing time to reach glass transition temperature (180 °C) and pyrolysis temperature (250 °C) at reverse side of the laminate. Moreover, these ceramic coatings could have provided better thermal barrier performance if these coating completely covered the surface and these were no holes on the surface from where heat could penetrate through the surface, which is subject of a forthcoming publication. The thermal barrier effect in future work will be studied at selected heat fluxes in absence of an ignition source. Alternative coating techniques such as sol–gel and layer-by-layer are also being explored.

References

[1] Schultz U, Leyens C, Fritscher K, Peters M, Saruhan-Brings B, Lavigne O, et al. Some recent trends in research and technology of advanced thermal barrier coating. Aerosp Sci Technol 2003;7:73–80.

[2] Jones RL. Thermal barrier coatings. In: Stern KH, editor. Metallurgical and ceramic protective coatings. UK: Chapman & Hall; 1996. p. 194–235.

[3] Evans AG, Mumm DR, Hutchinson JW, Meier GH, Pettit FS. Mechanisms controlling the durability of thermal barrier coatings. Prog Mater Sci 2001;46:505–53.

[4] Itoh Y, Saitoh M, Tamura M. Characteristics of MCrAlY coatings sprayed by high velocity oxygen-fuel spraying system. J Eng Gas Turbines Power 2000;122:43–9.

[5] Vuoristo P, Ahmaniemi S, Tuurna S, Mantyla T, Cordano E, Fignino F, Gualco GC. Development of HVOF sprayed NiCoCrAlYRe coatings for use as bond coats of plasma sprayed thermal barrier coatings. In: Proceedings of the ITSC 2002 – International thermal spray conference and exposition, Germany, 2002. p. 470–5.

[6] Sobolev VV, Guilemany JM, Nutting J. High velocity oxy-fuel spraying: theory, structure–property relationships and applications. UK: Maney Publishing; 2004. p. 3970.

[7] Chen Y, Liu W. Characterization and investigation of the tribological properties of sol–gel zirconia thin films. J Am Ceram Soc 2002;85(9):2367–9.

[8] Viazzi C, Bonino JP, Ansart F. Synthesis by sol–gel route and characterization of yttria stabilized zirconia coatings for thermal barrier applications. Surf Coat Technol 2006;201:3889–93.

[9] Kandola BK, Kandare E. Composites having improved fire resistance. In: Horrocks AR, Price D, editors. Advances in fire retardant materials. UK: Woodhead Publishers; 2008. p. 398–442.

[10] Kandare E, Kandola BK, Myler P, Edwards G. Thermo-mechanical responses of fiber-reinforced epoxy composites exposed to high temperature environments. Part I: Experimental data acquisition. J Compos Mater 2010;44:3093–114.

[11] Mouritz AP, Feih S, Kandare E, Mathys Z, Gibson AG, Des Jardin P, et al. Review of fire structural modelling of polymer composites. Compos. Part A: Appl. Sci. Manuf. 2009;40:1800–14.

[12] Mouritz AP, Gibson AG. Fire properties of polymer composite materials. Netherlands: Springer; 2006.

[13] Kandola B, Pornwannachai W. Enhancement of passive fire protection ability of inorganic fire retardants in vinyl ester resin using glass frit synergists. J Fire Sci 2010;28:357–81.

[14] Burzo M, Komarov P, Raad P. Thermal transport properties of gold-covered thin-film silicon dioxide. IEEE CPMT 2003;26:80–8.

[15] Hass DD, Zhao H, Dobbins T, Allen AJ, Slifka AJ, Wadley HNG. Multi-scale pore morphology in vapor deposited yttria-stabilized zirconia coatings. Mater Sci Eng A – Struct 2010;527:6270–82.

[16] Recoxit (Ohcera. Co., Ltd.), Technical specification data sheet. <http://www.ohcera.co.jp/pdf/Characteristics_of_RECOXIT.pdf> (downloaded on 18/06/2014).

[17] Image J Image processing and analysis in JAVA. The Programmer's Reference Guide v1.46d: <http://imagej.nih.gov/ij/macros/> (date: 28/11/2013).

[18] Biswas B, Kandola BK. The effect of chemically reactive type flame retardant additives on flammability of PES toughened epoxy resin and carbon fiber-reinforced composites. Polym Adv Technol 2011;22(7):1192–204.

[19] Kandola BK, Bhatti W, Kandare E. A comparative study on the efficacy of varied surface coatings in fireproofing glass/epoxy composites. Polym Degrad Stab 2012;97:2418–27.

[20] Everson K, Chukwunonso AK, Kandola BK. The effect of fire-retardant additives and a surface insulative fabric on fire performance and mechanical property retention of polyester composites. Fire Mater 2011;35:143–55.

[21] Wang X, Hu Y, Song L, Xing W, Lu H, Lv P, et al. Flame retardancy and thermal degradation mechanism of epoxy resin composites based on a DOPO substituted organophosphorus oligomer. Polymer 2010;51:2435–45.

[22] Schartel B, Hull TR. Development of fire-retarded materials—interpretation of cone calorimeter data. Fire Mater 2007;31:327–54.

[23] Koo JH, Ng PS, Cheung FB. Effect of high temperature additives in fire resistant materials. J Fire Sci 1997;15:488–504.

[24] Padture NP, Gell M, Jordan EH. Thermal barrier coatings for gas-turbine engine applications. Science 2002;296:280–4.

[25] Schartel B, Braun U, Schwarz U, Reinemann S. Fire retardancy of polypropylene/flax blends. Polymer 2003;44:6241–50.